Identification of a Shaft Thermal Bow by Means of Model-based Diagnostic Techniques

Andrea Vania[1], Paolo Pennacchi[1] and Steven Chatterton[1]

[1]Politecnico di Milano, Dept. of Mchanical Engineering
Via La Masa, 1, 20156 Milano, Italy
{Andrea.Vania, Paolo.Pennacchi, Steven.Chatterton}@polimi.it

Abstract

The most important faults of rotating machines can be modelled by means of proper sets of equivalent excitations having a suitable harmonic content. Therefore, mathematical models of rotating machines can be used by fault identification techniques that compare the experimental vibration data to the corresponding theoretical response of the rotor-system caused by a specific set of excitations. Unfortunately, several different faults can cause similar symptoms in the vibration of large rotating machines and, in the common case of flexible rotors, only a well-tuned model is able to provide reliable fault identifications. This paper shows the results of a study in which the cause of the abnormal vibration of the generator of a power unit has been investigated considering different types of fault. A thermal bow of the generator rotor has shown to be able to fit the simulation of the experimental transient vibrations. The diagnostic strategy used to investigate this case study can be applied to identify many other types of faults in rotating machines.

1 Introduction

Many faults and malfunctions in rotating machines can be detected by means of the analysis of the harmonic content of shaft and support vibrations. The trend analysis of magnitude and phase of the most important harmonic components of the frequency spectrum of the machine vibration, measured in operating condition, can give very important information. However, essential diagnostic indications can be obtained only by means of the analysis of the vibration data collected during machine runups and rundowns. Unfortunately, some different faults can give rise to similar symptoms in the machine vibration, therefore, also process and system parameters should be taken into account in the diagnostic analyses.

Fault symptom analysis techniques can detect impending faults and malfunctions and they can recognize the fault typology. However, these diagnostic methods are often unable to localize the fault and provide reliable estimates of its severity. These information are very important for prognostic analyses and predictive maintenance.

Mathematical models of the rotor-system can simulate and predict the machine vibration caused by many types of excitations. Moreover, the rotating machine faults give rise to dynamic forces and moments, having a characteristic harmonic content, which, in turn, cause shaft and support vibrations. Therefore, model-based diagnostic techniques can be used to simulate the machine dynamic behaviour caused by many faults and malfunctions as the most important faults can be modelled by means of proper sets of equivalent excitations having a suitable harmonic content. The same machine model can be used also by fault identification techniques that compare the experimental vibration data to the corresponding theoretical response of the rotor system caused by a specific set of excitations. These methods identify the most likely fault, included in a pre-established list of typical faults, by evaluating the set of equivalent excitations that minimizes the error between experimental data and numerical results. Diagnostic methods can also identify the location and severity of the fault. Therefore, the results provided by these techniques are very useful also to carry out a prognosis and study corrective actions. In the past, the authors of this paper developed some diagnostic and prognostic methods aimed at investigating faults in rotating machines. These model-based techniques are described in detail in [1].

This paper shows the results of a study in which the cause of the abnormal vibration of the generator of a power unit has been investigated. The results obtained considering different types of faults are shown and compared. A thermal bow of the generator rotor, compatible with physical phenomena that can affect the

shaft when it is subjected to different thermal states, has shown to be able to successfully simulate the 1 × rev. (1X) experimental transient vibration of the generator.

2 Brief theoretical background

In general, a model composed of beam Finite Elements is used to describe the mechanical properties of the shaft-train while the dynamic effects caused by fluid-film journal bearings and rolling element bearings are modelled by means of dynamic stiffness coefficients [1]-[4]. In the case of sleeve journal bearings the linearized coefficients of the fluid-film depend on the shaft rotational speed. In the end, some different methods can be used to model the mechanical characteristics of the foundation structure [5]. Then, the equation of motion of the rotating machine can be expressed in the following general form:

$$\left[\mathbf{M}\right]\ddot{\mathbf{x}} + \left(\left[\mathbf{C}(\Omega)\right] + \left[\mathbf{G}(\Omega)\right]\right)\dot{\mathbf{x}} + \left[\mathbf{K}(\Omega)\right]\mathbf{x} = \mathbf{F} \tag{1}$$

where Ω is the shaft angular velocity and $\mathbf{x}$ is the vector that contains the translational and angular displacements associated with the degrees of freedoms (d.o.f.s) of shafts and foundation. The mass, stiffness and damping matrices $\left[\mathbf{M}\right], \left[\mathbf{K}\right]$ and $\left[\mathbf{C}\right]$ describe the dynamic effects of the whole rotating machine while the matrix $\left[\mathbf{G}(\Omega)\right]$ takes into account the gyroscopic effects of the shaft-train. In the end, the vector $\mathbf{F}$ contains the dynamic excitations applied to the shaft-train.

By assuming that all the terms of the vector $\mathbf{F}$ are harmonic functions having the same frequency, $f_j = j\,\Omega / 2\,\pi$, with $\Omega_j = j\,\Omega$, we have:

$$\mathbf{F}(t) = \mathbf{F}_{0j}\, \mathrm{e}^{\mathrm{i}\,\Omega_j t} \tag{2}$$

where the vector $\mathbf{F}_{0j}$ contains complex terms. If the non-linear effects in the dynamic behavior of the rotor system can be neglected, the steady state response can be easily evaluated in the frequency domain. The steady state theoretical response is given by:

$$\mathbf{x}(t) = \mathbf{X}_{0j}\, \mathrm{e}^{\mathrm{i}\,\Omega_j t} \tag{3}$$

where the terms contained in the vibration vector $\mathbf{X}_{0j}$ are complex. For the shaft angular velocity Ω_k the eq.(1) can be rewritten as:

$$\left[\mathbf{B}\left(\Omega_k, \Omega_j\right)\right]\mathbf{x} = \mathbf{F} \tag{4}$$

Therefore, the vector $\mathbf{X}_{0j}\left(\Omega_j\right)$ of the theoretical vibrations can be expressed as:

$$\mathbf{X}_{0j}\left(\Omega_j\right) = \left[\mathbf{H}\left(\Omega_k, \Omega_j\right)\right]\mathbf{F}_{0j}\left(\Omega_j\right) \tag{5}$$

where the matrix $\mathbf{H}$ is the inverse of the matrix $\mathbf{B}$, while also the rotor-system excitations, like those caused by shaft unbalances, can depend on the shaft angular velocity.

Fault identification methods often consider a complex vector $\mathbf{X}_{th}$ in which the vibration vectors $\mathbf{X}_{0j}\left(\Omega_j\right)$, obtained for *N* different shaft angular velocities, Ω_k, are ordered in the following form:

$$\mathbf{X}_{th}^{\mathrm{T}} = \left\{ \mathbf{X}_{0j}^{\mathrm{T}}\left(\Omega_1\right),\ \mathbf{X}_{0j}^{\mathrm{T}}\left(\Omega_2\right), \ldots, \mathbf{X}_{0j}^{\mathrm{T}}\left(\Omega_N\right) \right\} \tag{6}$$

The vector $\mathbf{X}_{th}$ is generated considering the theoretical vibrations evaluated only at the measurement points with which the rotating machine is equipped. Similarly, the corresponding experimental vibrations can be included in the vector $\mathbf{X}_{exp}$ as:

$$\mathbf{X}_{exp}^{\mathrm{T}} = \left\{ \mathbf{X}_{exp,j}^{\mathrm{T}}\left(\Omega_1\right),\ \mathbf{X}_{exp,j}^{\mathrm{T}}\left(\Omega_2\right), \ldots, \mathbf{X}_{exp,j}^{\mathrm{T}}\left(\Omega_N\right) \right\} \tag{7}$$

where the vector $\mathbf{X}_{exp,j}^{\mathrm{T}}\left(\Omega_j\right)$ contains the harmonic component of the experimental vibrations associated with the frequency $f_j = j\,\Omega_k / 2\,\pi$, measured for a shaft angular velocity Ω_k. Then, considering eq.(5) and eq.(6) it is possible to write the following expression:

$$\left\{\begin{array}{c}\mathbf{X}_{0j}\left(\Omega_1\right)\\ \cdots\\ \mathbf{X}_{0j}\left(\Omega_N\right)\end{array}\right\}=\left[\begin{array}{c}\mathbf{H}\left(\Omega_1\right)\\ \cdots\\ \mathbf{H}\left(\Omega_N\right)\end{array}\right]\left\{\begin{array}{c}\mathbf{F}_{0j}\left(\Omega_1\right)\\ \cdots\\ \mathbf{F}_{0j}\left(\Omega_N\right)\end{array}\right\} \tag{8}$$

That is:

$$\mathbf{X}_{th}=\left[\mathbf{A}\right]\mathbf{F}_{0j} \tag{9}$$

The equivalent excitations $\mathbf{F}_{0j}$, applied to pre-established axial positions of the shaft-train, which cause the best fit between experimental vibrations and numerical results can be obtained by solving the following problem:

$$\left[\mathbf{A}\right]\mathbf{F}_{0j}=\mathbf{X}_{exp} \tag{10}$$

In general, the problem expressed by eq.(10) is over-determined being the number of rows of the matrix $\left[\mathbf{A}\right]$ larger than the number of the unknowns contained in the excitation vector $\mathbf{F}_{0j}$. Therefore, Least Squares Error Methods can be used to estimates the equivalent excitations that minimize the square error, ε, often called residual, between experimental data and theoretical response, given by:

$$\varepsilon = \left(\mathbf{X}_{th}^{\mathrm{T}}-\mathbf{X}_{exp}^{\mathrm{T}}\right)^{*}\left(\mathbf{X}_{th}-\mathbf{X}_{exp}\right) \tag{11}$$

where the symbol * indicates complex conjugate quantities.

Similarly, the equivalent excitations $\mathbf{F}_{0j}$ can be estimated by maximizing the Coherence Factor, γ, between the two vectors $\mathbf{X}_{exp}$ and $\mathbf{X}_{th}$, expressed as:

$$\gamma = \frac{\left|\left(\mathbf{X}_{exp}^{*}\right)^{\mathrm{T}}\left(\mathbf{X}_{th}\right)\right|^2}{\left(\left(\mathbf{X}_{exp}^{*}\right)^{\mathrm{T}}\left(\mathbf{X}_{exp}\right)\right)\left(\left(\mathbf{X}_{th}^{*}\right)^{\mathrm{T}}\left(\mathbf{X}_{th}\right)\right)} \tag{12}$$

For a given type of fault the axial position of the equivalent excitations $\mathbf{F}_{0j}$ can be automatically varied by the fault identification method. Moreover, different types of faults, with which different sets of equivalent excitations are associated, can be considered. The most likely fault is that which causes the lowest residual ε and the highest Coherence Factor γ.

3 Case study

The machine-train of the power unit considered in this paper was composed of a high-pressure-intermediate-pressure (HP-IP) steam turbine, a low-pressure (LP) turbine and a generator. These machines were connected by means of rigid couplings. The machine-train diagram and the bearing numbers are shown in Figure 1, while a more detailed drawing of the generator rotor is shown in Figure 2. The rated power of this unit was 175 MW while the operating speed was 3000 rpm.

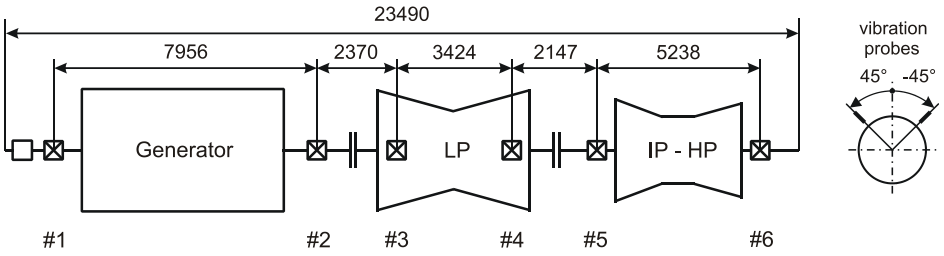

Figure 1: Machine-train diagram and support numbering

Each support was equipped with a pair of XY proximity probes, oriented 90 degrees apart (Figure 1), which measured the shaft-to-support relative vibration. Moreover, a pair of seismic transducers, mounted on the same measurement points of the proximity probes, measured the support absolute vibration. Therefore, the absolute vibration of the shaft could be easily obtained.

Some maintenance activities were performed on the generator during a long planned outage. This maintenance required to dismount the two rotor caps, located at the ends of the active part of the generator rotor, and to machine the flange of the coupling facing the LP turbine.

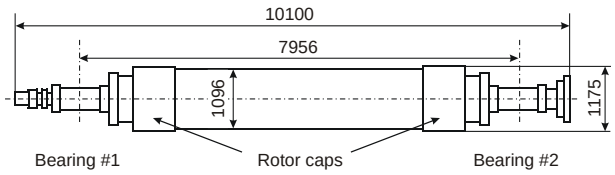

Figure 2: Generator rotor

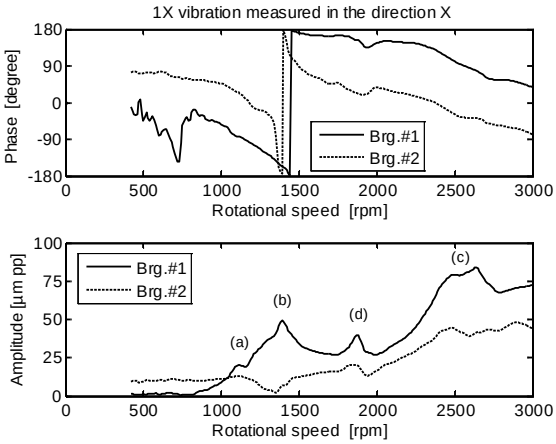

Figure 3: 1X absolute vibrations measured at bearing #1 during a runup occurred before the maintenance of the generator

Figure 3 shows the 1X absolute vibration of the generator measured at bearing #1 during a runup carried out before the maintenance. Owing to the oil-film anisotropy the first balance resonance was split in two flexural critical speeds, close to 1075 rpm and 1365 rpm, respectively, which caused the amplitude peaks indicated with the letters (a) and (b) in Figure 3. The resonance peak indicated with the letter (c), in the same figure, close to 2640 rpm, is caused by a shaft resonance associated with a typical second bending normal mode in which the vibrations measured at the opposite ends of the rotor are out-of-phase. In the end, the amplitude peak close to 1870 rpm, indicated with the letter (d) in Figure 3, is caused by a natural frequency of the foundation structure.

The amplitude of the 1X vibration of the generator measured before the maintenance were not very high, either when passing through the critical speeds and at the operating speed. This indicates that, before the maintenance, the residual unbalance of the generator was not excessive and also the shaft bow was rather limited.

The shape of the vibration normal modes of the generator associated with the above mentioned critical speeds has been studied by means of a mathematical model of the rotor system. Figure 4 shows the Finite Element model of the shaft-train composed of 108 beam FEs. This machine model included also the linearized coefficients of the oil-film dynamic stiffness of the journal bearings that support the shafts and the

basic mechanical characteristics of the foundation structure. The techniques used to model the fully assembled rotating machine are described in [2]-[4]. Figure 5 shows the numbering of some important nodes of the FE model of the generator rotor.

Figure 4: Finite Element Model of the machine-train

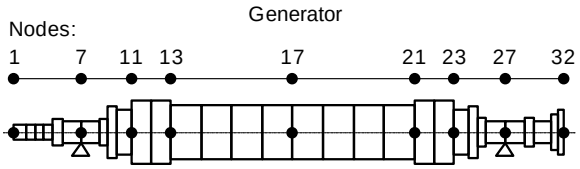

Figure 5: Important nodes of the generator model

The experimental estimates of the flexural critical speeds of the generator contained in the range below the operating speed are compared in Table 1 to the corresponding numerical results provided by an eigenvalue analysis of the machine model. The accordance between experimental values and numerical results is satisfactory. Figure 6 shows the shape of the vibration normal modes associated with the first three critical speeds of the generator rotor.

The typical first bending normal modes associated with the first two critical speeds contained in the range close to 1200 rpm show a maximum vibration amplitude in the middle of the span between the generator supports #1 and #2. Conversely, the bending normal mode associated with the critical speed close to 2700 rpm is characterized by out-of-phase vibrations at the two generator supports, while very low vibration levels occur in the middle of the span between the two supports. This is the shape of a typical second normal mode of many shafts mounted on two supports.

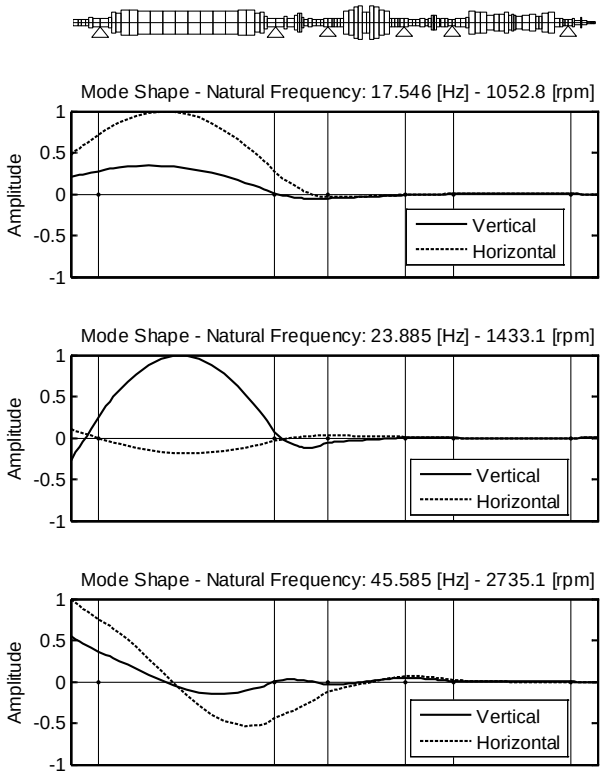

Figure 6: First three normal modes of the generator rotor

At the end of the maintenance the generator rotor was not subjected to any balancing activity as the manufacturer considered it unnecessary. Unfortunately, since the first runup performed after the machine outage, the 1X vibration of the generator showed very high levels when passing through the first balance resonance, especially at bearing #1.

FLEXURAL CRITICAL SPEEDS	
Experimental	Theoretical
1075 rpm	1053 rpm
1365 rpm	1433 rpm
2640 rpm	2735 rpm

Table 1: Comparison between experimental and theoretical flexural critical speeds

The plain curves illustrated in Figure 7 and in Figure 8 show the 1X absolute vibration of the shaft measured at bearings #1 and #2, in the X direction, during a reference runup. The maximum amplitude of the vibration measured at bearing #1 reaches 265 μm pp at 1370 rpm. Conversely, the generator vibration measured in the rotational speed range from 2000 rpm to 3000 rpm was lower than 80 μm pp at any measurement point. This dynamic behaviour showed to be repeatable during further machine runups.

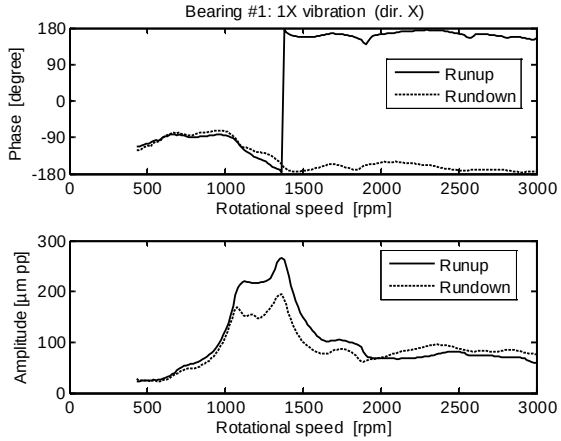

Figure 7: 1X absolute vibration measured at bearing #1, in the X direction, during a runup and a rundown

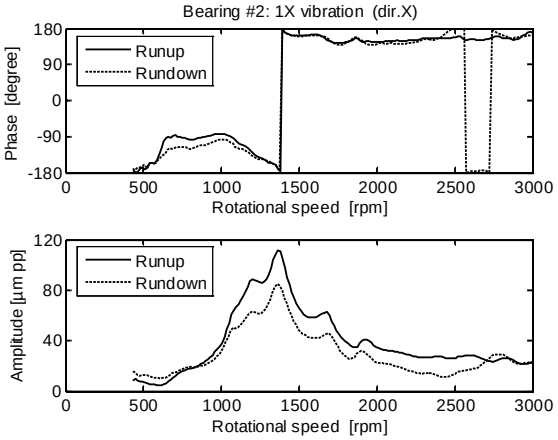

Figure 8: 1X absolute vibration measured at bearing #2, in the X direction, during a runup and a rundown

A model-based diagnostic analysis performed by the authors showed that the most likely cause of the very high 1X vibration of the generator that occurred in the speed range from 1000 rpm to 1600 rpm was the presence of two local unbalances located in the shaft area close to each rotor cap, that is at nodes #13 and #21 of the shaft model (Figure 5). The results of this fault identification, performed by means of model-based methods, are shown and discussed in [6]. The two identified unbalances, located at the nodes #13 and #21, that is at the opposite ends of the shaft, have a similar magnitude and a similar phase: 0.8902 kgm @ 349° and 0.8383 kgm @ 353°, respectively. Therefore, these unbalances excite the first bending normal mode of generator rotor very much while the energy introduced in the rotational speed range above 2300 rpm, highly dominated by the dynamic effects of the second normal mode of the rotor, is rather small. In fact, in the above mentioned speed range, the centrifugal forces caused by the two unbalances are rather similar and nearly in-phase while the shaft displacements where they are applied have a similar magnitude but opposite sign.

This behaviour is also confirmed by comparing the generator 1X vibrations illustrated in Figures 3, 7 and 8. It is possible to note that, after the maintenance, the resonance peak close to 2600 rpm that was quite evident before the machine outage, is almost absent. This behaviour is in accordance to the assumed axial and angular position of the two local unbalances as well as to the shape of the second bending normal mode of the generator.

Since only few start-ups of the unit were carried out during a year, and sufficiently low vibration levels occurred in the operating condition, it was decided to postpone the optimization of the residual unbalance of the generator to the next planned maintenance. However, the monitoring data collected during several months after the maintenance showed that, in the rotational speed range close to the first balance resonance, the generator vibration measured during the rundowns was rather different from that measured during the runups. This induced to suspect that the generator was affected by a secondary minor malfunction, the effects

of which on the shaft dynamic behaviour depended on the machine thermal state. The dashed curves illustrated in Figures 7 and 8 show the 1X absolute vibrations of the generator rotor measured at bearings #1 and #2, respectively, during a reference rundown.

Then, a model-based diagnostic analysis was carried out to investigate the cause of this phenomenon. The non-linear effects in the machine vibration were arbitrarily considered not very important. Therefore, the additional 1X absolute vibration of the generator that can be ascribed to the secondary malfunction were evaluated, at each rotational speed, by subtracting the 1X vibration vector measured during the rundown from the corresponding 1X vector measured during the runup. Figure 9 shows the amplitude of these additional vibration evaluated at bearings #1 and #2 in the direction X.

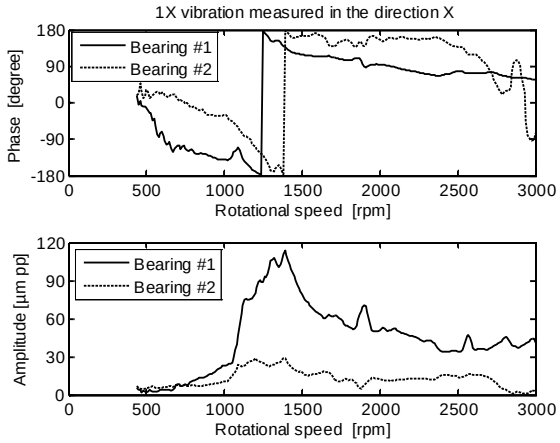

Figure 9: 1X additional absolute vibration of the shaft measured at bearings #1 and #2, in the X direction

4 Shaft bow identification

On the basis of the characteristics of generator vibrations it was suspected that the dynamic behaviour shown in Figure 9 was caused by a shaft thermal bow that, on generators, is not unusual owing to the phenomena due to rotor current and shaft temperature that often affect the rotor windings.

The dynamic effects of shaft thermal bows can be simulated by applying a pair of opposite bending moments to different cross-sections of the shaft model ([7][8]). Therefore, these moments rotate with the shaft causing 1X harmonic excitations. In general, two bending moments applied to narrow cross-sections of the rotor cause a local bow while an extended bow can be simulated by applying the pair of opposite moments to distant nodes of the finite element model of the shaft.

In this investigation, the magnitude and the axial and angular position of the two bending moments that are able to simulate the experimental 1X additional vibration of the generator were unknown. These equivalent excitations have been identified by means of a model-based method whose theoretical background is described in detail in [1]. In general, the excitations, applied to the shaft-train model, which simulate the actual fault, are identified by minimizing an objective function based on the error between the experimental vibration data and the numerical response of the rotor system.

Let us denote by i and j the nodes of the finite element model of the shaft to which the two opposite bending are applied. In the fault identification process these two nodes have been varied from the rotor cap mounted on the Non-Drive-End (NDE) of the generator and the rotor cap mounted on the opposite end. That is from node #11 to node #23 of the generator model shown in Figure 5. In this way, both local and extended shaft bows can be simulated.

The minimum residual, $\varepsilon = 0.2130$, and then the maximum coherence factor, $\gamma = 0.7871$, were obtained by applying two opposite bending moments to the nodes #11 and #23, that is to the outboard ends of the opposite rotor caps where the rotor windings are locked (Figure 5). The magnitude of the identified moments is 26.931 kNm while the corresponding phases are 285° and 105° degree. Figures 10 and 11 show the comparison between the 1X experimental additional vibrations of the generator measured at bearings #1 and #2, respectively, and the corresponding theoretical vibrations caused by the identified bending moments. The fitting between experimental data and numerical results is satisfactory.

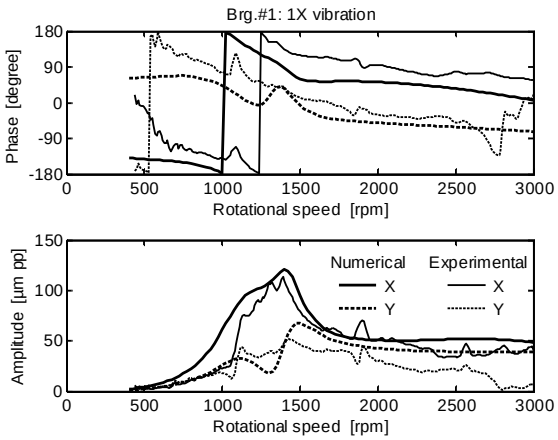

Figure 10: 1X additional vibration evaluated at bearing #1: comparison between experimental data and predicted vibrations caused by the identified shaft-bow

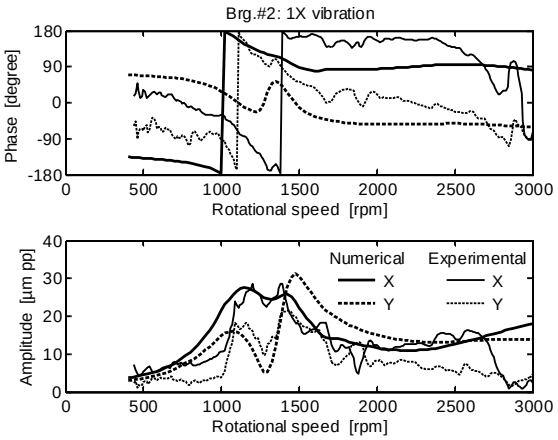

Figure 11: 1X additional vibration evaluated at bearing #2: comparison between experimental data and predicted vibrations caused by the identified shaft-bow

Figure 12 shows the map of the coherence factors, γ, evaluated by the fault identification method by varying the pairs of nodes *i* and *j* of the generator model to which the bending moments are applied. The values of γ marked with a circle are fictitious, i.e. false values, as they correspond to pairs of opposite bending moments applied to a same node: this nullifies the effects of these excitations. Conversely, the bold curve reported in Figure 12 joints the coherence factor values obtained by moving the pair of nodes *i* and *j* from the opposite rotor caps to the middle of the span between the supports #1 and #2. The section of the map of Figure 12 along the bold curve is reported in Figure 13.

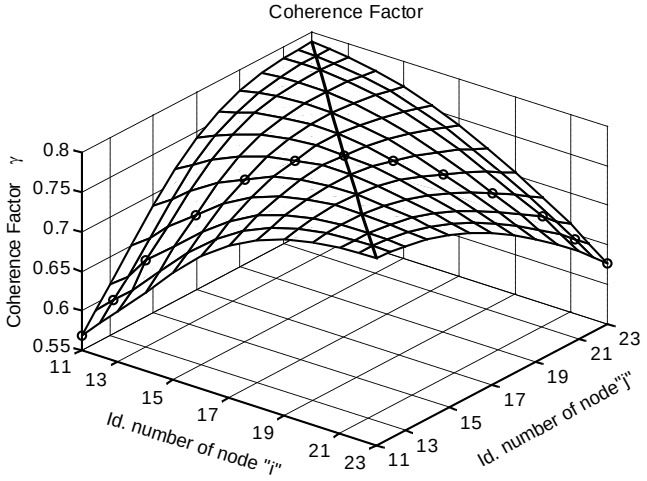

Figure 12: Shaft bow identification: Coherence Factor map

It is evident that local bows, e.g. caused by local defects of the rotor winding insulation ([9]), simulated by applying the two bending moments to narrow cross-sections of the shaft, cause low values of the coherence factor between experimental data and numerical results. Only local bows located in the middle of the span between the generator supports are able to cause a satisfactory fitting of the experimental data. However, since no electrical defect was detected, it is more likely that the generator heating caused by the rotor current that flows in the operating condition caused a not axial-symmetric temperature distribution of the shaft and then an extended shaft thermal bow. Also unequal axial expansions of the copper bars mounted into slots located in opposite diametrical positions of the generator rotor can cause similar effects.

Figure 14 shows the magnitude of the best pair of bending moments evaluated by applying a moment to the node #11 and by varying the axial position of the opposite moment from node #12 to node #23. Local

bows localized in the shaft area close to the outboard rotor cap cause a considerable increase of the bending moment magnitude.

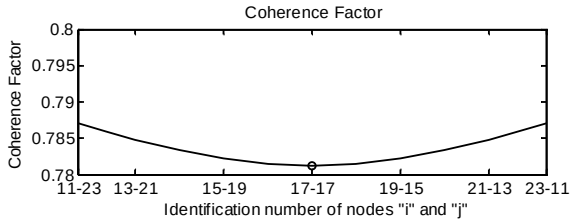

Figure 13: Coherence Factor associated with bending moments applied to the pair of nodes aligned along the bolded line shown in Figure 13

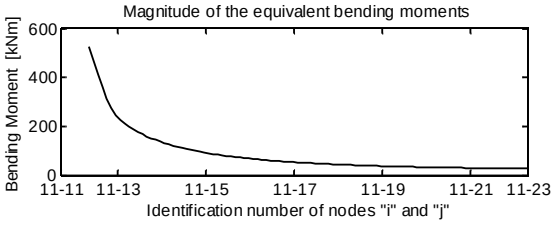

Figure 14: Influence of the axial position of the equivalent excitations on the magnitude of the identified bending moments

5 Unbalance identification

A shaft bow is not the only fault that can cause the considerable difference of the generator dynamic behavior that occurred between runups and rundowns. In fact, also a residual unbalance can cause abnormal 1X vibrations.

Therefore, in order to validate the fault identification previously described, in which a shaft thermal bow has been assumed to be the cause of the unusual dynamic behavior of the generator, it was decided to carry out a study in which the fault has been assumed to be a local residual unbalance. This type of fault is modeled by means of a simple unbalance applied to a single node of the generator finite element model.

The procedure used to identify the unbalance that minimizes the error between experimental vibrations and numerical results is similar to that used for the previous investigation. In this study the axial position of the unbalance was varied from node #1 to node #32, that is from the outboard end to the inboard end of the of the generator rotor. The minimum residual, $\varepsilon = 0.4555$, and then the maximum coherence factor, $\gamma = 0.5445$, were obtained by applying a local unbalance to the node #16 (Figure 5), that is in an area of the rotor that is close to the middle of the span between the supports #1 and #2. The magnitude of the identified unbalance is 0.6088 kgm while the corresponding phase is 313°.

Figure 15 shows the comparison between the 1X experimental additional vibrations of the generator measured at bearing #1 and the corresponding theoretical vibrations caused by the identified unbalance. The residual obtained with this analysis is more than double in comparison to that obtained considering a shaft bow as the fault by which the generator is affected. According to this, the coherence factor γ associated with this study is rather low.

Figure 16 shows the influence of the unbalance axial position on the coherence factor γ. It is evident that unbalances applied to rotor areas that are not very close to the middle of the span between the generator supports cause very low values of the coherence factor γ. This is due to the fact that only unbalances applied close to the centre of the rotor are unable to excite considerably the second bending mode of the generator, associated with a critical speed close to 2600 rpm. Conversely, the levels of the 1X additional vibrations of the generator measured in the rotational speed range above 2300 rpm are rather low. Figure 17 shows the influence of the fault axial position on the imbalance magnitude.

In the end, Figure 18 shows the influence of the unbalance axial position on the amplitude of the absolute vibration of the shaft evaluated at bearing #1 in the X direction. When the rotational speed exceeds 2300 rpm, the increasing magnitude of the centrifugal force due to the unbalance and the excitation of the second bending mode of the generator cause evident dynamic effects in the shaft vibration, especially when the unbalance is applied to some particular areas of the rotor. Conversely, when the unbalance is applied to nodes that are close to the opposite ends of the generator, the first balance resonance is very weakly excited.

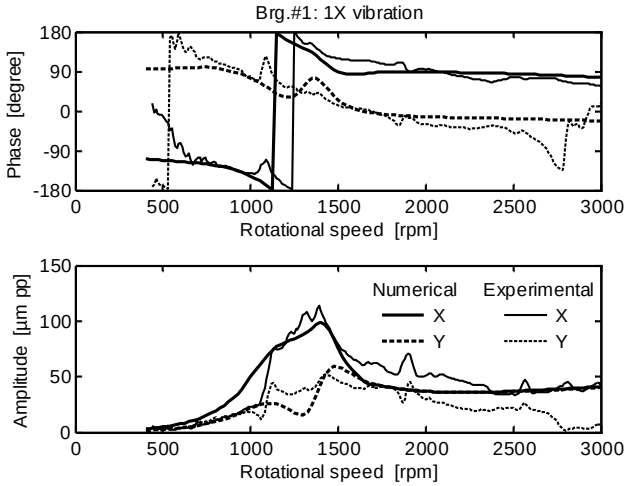

Figure 15: 1X additional vibration evaluated at bearing #1: comparison between experimental data and predicted vibrations caused by the identified unbalance

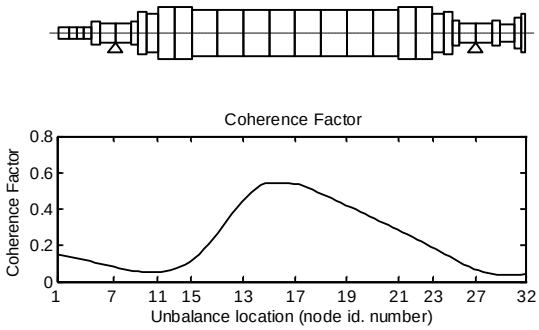

Figure 16: Influence of the fault axial position on the Coherence Factor

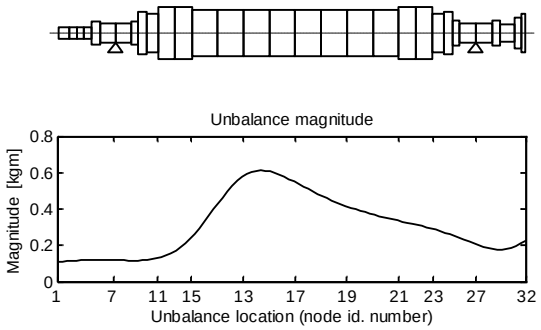

Figure 17: Influence of the fault axial position on the unbalance magnitude

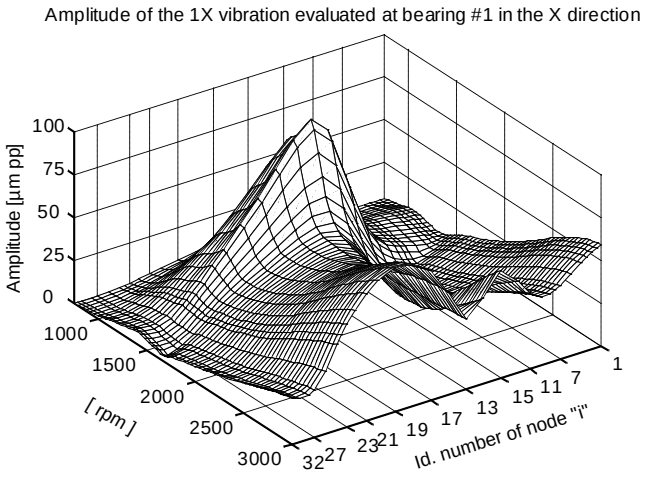

Figure 18: Map of the amplitude of the 1X vibration evaluated at bearing #1, in the X direction, by varying the axial position of the shaft unbalance

6 Fault identification

The vibration data reported in Figures 7 and 8 show that the dynamic behavior of the generator was affected by the machine thermal state. The presence of a local unbalance applied in the middle of the shaft, the magnitude of which must change with the temperature, is less likely than the presence of an extended thermal bow of the shaft. This assumption, based on the experience and the knowledge of physical phenomena that commonly affect the generator rotor, is confirmed also by the important difference between the values of the coherence factor γ obtained with the two investigations in which the above mentioned different faults have been considered.

The results obtained with this diagnostic strategy, based on the use of a machine model, can be very useful to determine appropriate maintenance actions aimed at eliminating the cause of the dynamic excitation that induced the sensitivity of the generator vibration to the machine thermal state.

7 Conclusions

This paper has shown the results of a study in which the cause of the abnormal vibration of the generator of a power unit has been investigated. The results obtained considering different types of faults are shown and compared. The most likely fault, that is a shaft thermal bow, has been determined by applying model-based techniques that minimize the error between the experimental vibrations of the rotating machine and the corresponding theoretical response. The possible machine faults have been simulated by means of suitable sets of equivalent excitations that are applied to some nodes of the finite element model of the shaft-train.

The diagnostic strategy used to identify the cause of the abnormal vibration of the generator has shown to be able to recognize the type of the fault as well as to evaluate severity and location of the fault. This diagnostic procedure can be applied to identify many other types of faults in rotating machines.

References

[1] N. Bachschmid, P. Pennacchi, A. Vania, *Identification of multiple faults in rotor systems*, Journal of Sound and Vibration, 254, No. 2, University Press (2002), pp.327-366.

[2] R. Isermann, *Supervision, fault-detection and fault-diagnosis methods: an introduction*, Control Engineering Practice, Elsevier (1997), pp.639-652.

[3] M. Lalanne, G. Ferraris, *Rotordynamics Predictions in Engineering*, 1998, John Wiley & Sons Inc., Chichester, England.

[4] M. Adams, *Rotating machinery vibration*, 2001, Marcel Dekker Inc., New York, N.Y., USA.

[5] P. Pennacchi, N. Bachschmid, A. Vania, G. Zanetta, L. Gregori, *Use of Modal Representation for the Supporting Structure in Model Based Fault Identification of Large Rotating Machinery: Part 2 – Application to a Real Machine*, Mechanical System and Signal Processing, Vol. 20, No. 3, 2006, pp. 682-701.

[6] A. Vania, P. Pennacchi, S. Chatterton, *Effects of the shaft normal modes on the model-based identification of unbalances in rotating machines*, Proc. of ASME Turbo Expo 2011, GT2011-46184, June 6-10, Vancouver, Canada.

[7] P. Pennacchi, A. Vania, *Accuracy in the Identification of a Generator Thermal Bow*, Journal of Sound and Vibration, Vol. 274, No. 1-2, 2004, pp.273-295.

[8] P. Pennacchi, A. Vania, *Analysis of the Shaft Thermal Bow Induced by Rotor-to-Stator Rubs*, IASME Transactions, Vol. 1, No. 1, 2004, pp.193-198.

[9] G. Klempner, I. Kerszenbaum, *Operation and Maintenance of Large Turbo-Generators*, 2004, John Wiley & Sons Inc, Piscataway, USA.